Mixing and ozone loss in the 1999–2000 Arctic vortex: Simulations with the three-dimensional Chemical Lagrangian Model of the Stratosphere (CLaMS)

Paul Konopka,[1] Hildegard-Maria Steinhorst,[1] Jens-Uwe Grooß,[1] Gebhard Günther,[1] Rolf Müller,[1] James W. Elkins,[2] Hans-Jürg Jost,[3] Erik Richard,[2] Ulrich Schmidt,[4] Geoffrey Toon,[5] and Daniel S. McKenna[6]

[1] The three-dimensional (3-D) formulation of the Chemical Lagrangian Model of the Stratosphere (CLaMS-3d) is presented that extends the isentropic version of CLaMS to cross-isentropic transport. The cross-isentropic velocities of the Lagrangian air parcels are calculated with a radiation module and by taking into account profiles of ozone and water vapor derived from a HALOE climatology. The 3-D extension of mixing maintains the most important feature of the 2-D version as mixing is mainly controlled by the horizontal deformations of the wind fields. In the 3-D version, mixing is additionally driven by the vertical shear in the flow. The impact of the intensity of mixing in the 3-D model formulation on simulated tracer distributions is elucidated by comparing observations of CH_4, Halon-1211, and ozone from satellite, balloon, and ER-2 aircraft during the SOLVE/THESEO-2000 campaign. CLaMS-3d simulations span the time period from early December 1999 to the middle of March 2000, with air parcels extending over the Northern Hemisphere in the vertical range between 350 and 1400 K. The adjustment of the CLaMS-3d mixing parameters to optimize agreement with observations was obtained for strongly inhomogeneous, deformation-induced mixing that affects only about 10% of the air parcels per day. The optimal choice of the aspect ratio α defining the ratio of the mean horizontal and vertical separation between the air parcels was determined to be 250 for model configuration with a horizontal resolution $r_0 = 100$ km. By transporting ozone in CLaMS-3d as a passive tracer, the chemical ozone loss was inferred as the difference between the observed and simulated ozone profiles. The results show, in agreement with previous studies, a substantial ozone loss between 380 and 520 K with a maximum loss at 460 K of about 1.9 ppmv, i.e., of over 60% locally, from December to the middle of March 2000. During this period, the impact of isentropic mixing across the vortex edge outweighs the effect of the spatially inhomogeneous (differential) descent on the tracer/ozone correlations in the vortex. Mixing into the vortex shifts the early winter reference tracer/ozone correlation to higher values, which may lead to an underestimate of chemical ozone loss, on average by 0.4 and 0.1 ppmv in the entire vortex and the vortex core, respectively. *INDEX TERMS:* 0340 Atmospheric Composition and Structure: Middle atmosphere—composition and chemistry; 0341 Atmospheric Composition and Structure: Middle atmosphere—constituent transport and chemistry (3334); 3334 Meteorology and Atmospheric Dynamics: Middle atmosphere dynamics (0341, 0342); *KEYWORDS:* stratosphere, Lagrangian transport, mixing, ozone loss, SOLVE/THESEO 2000, CLaMS

[1]Institute for Stratospheric Chemistry (ICG-I), Jülich, Germany.
[2]Aeronomy Laboratory, National Oceanic and Atmospheric Administration, Boulder, Colorado, USA.
[3]NASA Ames Research Center, Moffett Field, California, USA.
[4]Johann Wolfgang Goethe-University, Frankfurt am Main, Germany.
[5]Jet Propulsion Laboratory, Pasadena, California, USA.
[6]National Center for Atmospheric Research, Boulder, Colorado, USA.

1. Introduction

[2] Motivated by the the existence of filamentary structures in the stratospheric chemical tracer fields that are often below the spatial resolution of the highest-resolution Eulerian models, [*McKenna et al.*, 2002a, 2002b] formulated the isentropic version of the Chemical Lagrangian Model of the Stratosphere (CLaMS-2d) based on Lagrangian transport of tracers. The validation of CLaMS-2d was performed by

comparison with the experimental data from the SOLVE/THESEO-2000 campaign [*Newman et al.*, 2002]. In particular, the isentropic mixing, chemical ozone loss and the impact of mixing on the chlorine deactivation in the Arctic polar vortex were quantified [*Grooß et al.*, 2002; *Konopka et al.*, 2003].

[3] The main shortcoming of CLaMS-2d studies arises from the limited validity of its isentropic transport scheme that can be applied only over time periods when cross-isentropic velocities are negligible. In this paper we overcome this disadvantage by formulating in section 2 a full three-dimensional (3-D) generalization of CLaMS transport algorithm. To verify this scheme, section 3 describes tracer transport studies in the northern polar stratosphere between 1 December 1999 and 20 March 2000, i.e., for a time period when a significant subsidence of the vortex air masses was observed [*Greenblatt et al.*, 2002] and, consequently, a full 3-D description of transport is necessary.

[4] Unlike Eulerian CTMs, CLaMS considers an ensemble of air parcels (APs) on a time-dependent irregular grid. After initialization of the model, each of the following transport steps Δt consists of two parts: pure advection in terms of the trajectories and subsequent mixing. Mixing can be understood as a consequence of the numerical diffusion due to adaptive regridding and associated averaging of the APs. While the purely advective transport is completely reversible, the regridding procedure that is driven by the deformations in the flow, defines the amount of irreversibility (i.e., mixing) affecting the transport of the chemical constituents [*McKenna et al.*, 2002b].

[5] In particular, *McKenna et al.* [2002b] have shown that deformation-induced mixing in CLaMS-2d is mainly driven by the horizontal strain in the flow. We show in the next section that in the 3-D case, in addition to the horizontal strain, the vertical shear contributes to the deformations and, consequently, to mixing in the flow. Owing to a strongly inhomogeneous spatial distribution of such deformations, mixing in CLaMS only occurs at few places in the flow. The intensity of mixing is controlled by the extent of deformation over a critical value that is quantified in terms of the critical Lyapunov exponent λ_c and the time step Δt (or the regridding frequency $1/\Delta t$) [*McKenna et al.*, 2002b]. *Waugh et al.* [1997] used the concept of bulk diffusivity to describe the mean mixing properties of the flow and estimated its value to be of the order 10^3 m^2 s^{-1}. Mixing in CLaMS-3d generalizes this idea to a more realistic spatially and temporally inhomogeneous mixing. Furthermore, in contrast to the Eulerian approach where numerical diffusion is present everywhere in the flow domain, the contribution of the CLaMS regridding procedure to the transport can be continuously reduced until species are transported only along trajectories without any mixing between the APs.

[6] In addition to the parameters controlling the deformation-induced mixing (i.e., λ_c and Δt), the horizontal and vertical mixing processes between the APs are dependent on the mean horizontal and vertical separations which represent the approximate horizontal and vertical scales L_h and L_v resolved by the model. *Haynes and Anglade* [1997] argued that the averaged stratospheric value for the aspect ratio $\alpha = L_h/L_v$ is given by ≈ 250 and that α also approximates the ratio between the horizontal and vertical diffusivities D_h and D_v through $\alpha^2 = D_h/D_v$. Thus the horizontal separation r_0

between the APs and the aspect ratio α together with the critical Lyapunov exponent λ_c and the regridding frequency $1/\Delta t$ are the parameters governing mixing in the CLaMS-3d formulation.

[7] By comparing simulated tracer distributions of CH$_4$ and Halon-1211 with high-resolution observations, we determine in section 3 the optimal choice of the mixing parameters. To quantify the dilution of vortex air due to the transport of the midlatitude air across the vortex edge, an artificial tracer is initialized as 1 inside and 0 outside the vortex. Using high-resolution N$_2$O measurements on board the ER-2, *Jost et al.* [2002] found that between January and March 2000 over the potential temperature range 350–500 K, signatures of midlatitude air in the vortex were observed during 15% of the flight duration. Further, about 60% of these midlatitude events had a spatial extent of less than 13 km. We discuss in section 3 how far these statistics can be reproduced by CLaMS-3d simulations and the implications for the dilution of vortex air through intrusions of midlatitude air into the vortex.

[8] One key assumption in many efforts to quantify ozone loss in the polar vortex has been that there is negligible transport of midlatitude air across the polar vortex edge [e.g., *Müller et al.*, 1997; *Knudsen et al.*, 1998]. In the so-called "tracer correlation approach" (TRAC) a long-lived reference tracer (e.g., CH$_4$ or N$_2$O) is correlated with ozone in late fall and in the spring for air masses within a well-established polar vortex by using aircraft [e.g., *Proffitt et al.*, 1990; *Richard et al.*, 2001], balloon [e.g., *Müller et al.*, 2001; *Salawitch et al.*, 2002], or satellite observation [e.g., *Müller et al.*, 2002; *Tilmes et al.*, 2003]. Thus with the assumption that mixing does not significantly influence the chemical composition of the vortex air masses, the chemical ozone loss may be estimated by the difference in ozone between the late fall and spring for a given mixing ratio of a reference tracer.

[9] The polar vortex is generally considered to be a relatively isolated region of the stratosphere which forms in the early winter [*McIntyre and Palmer*, 1984]. However, the degree of isolation and the variability of the polar vortex varies from year to year. Studying the impact of mixing on nonlinear tracer-tracer correlations inside the vortex, *Plumb et al.* [2000] suggested that transport of midlatitude air into the vortex edge might confound attempts to use tracer-tracer relationships to estimate ozone loss. During the SOLVE/THESEO-2000 campaign, the small-scale structures in the high-resolution CH$_4$, N$_2$O time series could be traced back to intrusions of midlatitude air into the vortex [*Jost et al.*, 2002; *Konopka et al.*, 2003] and, consequently, indicated some mixing across the vortex edge. Based on balloon observations, *Ray et al.* [2002] suggested that in early vortex 1999 the spatially inhomogeneous descent rates within the vortex, the so-called differential descent, created horizontal gradients in long-lived tracers that were then mixed throughout the vortex over the course of the winter [*Plumb et al.*, 2003].

[10] Using CLaMS-3d with optimal mixing parameters, both the differential descent and mixing across the vortex edge may influence tracer transport realistically. Before evaluating the impact of mixing on the tracer/ozone correlations (section 5), we discuss the ozone loss in winter 2000 (section 4). Applying the method described by *Goutail et al.* [1999], we compare ozone transported with CLaMS-3d as a passive tracer with the aircraft- and balloon-borne in situ
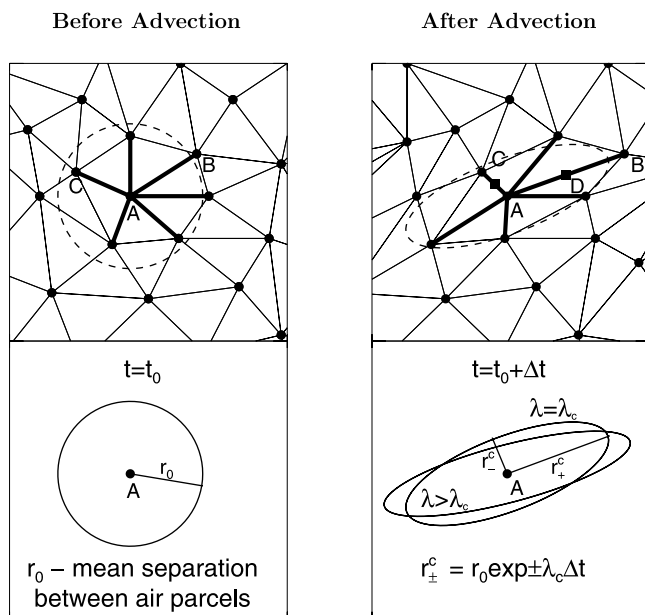
Figure 1. Deformation-induced mixing in CLaMS-2d [*McKenna et al.*, 2002b]. (left) The initial quasi-uniform distribution of APs (filled circles) with a mean separation between the APs given by r_0. Using the Delaunay triangulation, the nearest neighbors (NNs) of each AP are determined (e.g., thick lines connecting point A with its NNs). The circle with radius r_0 denotes the undeformed state of the grid. (right) After the advection step Δt, some parts of the grid can be deformed (i.e., the circle is deformed into an ellipse). Thus the relative distances from A to its NN change due to the flow-induced deformation; some APs like B move further away while some like C move closer. Using the critical Lyapunov exponent λ_c (free parameter) the critical horizontal separations $r_\pm^c$ are defined. If the distance AB exceeds r_+^c, then a new AP D is inserted midway between A and B (insertion), conversely, if the distance AC falls below a critical minimum separation r_-^c, then APs A and C are removed and a new grid point is introduced midway between the positions of A and C (merging). This numerical diffusion due to insertion and merging results in mixing in CLaMS-2d. It can be shown that highest mixing intensities (which are proportional to the number of the interpolations) occur in the grid regions with Lyapunov exponents λ exceeding λ_c where λ is derived from the elongation of a circle with radius r_0.

measurements. The passive ozone within CLaMS-3d offers a reliable reference to quantify ozone loss because its distribution is determined by transport that was validated by comparison with in-situ observations. Finally, in section 5, we study the effect of mixing on the tracer/ozone correlation and discuss the influence of this effect on the calculations of ozone loss. Section 6 discusses the results and presents our conclusions.

2. Three-Dimensional Generalization of the Transport Scheme

[11] A detailed description of the isentropic (2-D) Lagrangian transport scheme is given by *McKenna et al.*

[2002b]. Here, we recapitulate only the salient features of CLaMS-2d: An ensemble of APs is initialized on an isentropic level (θ = const, θ-potential temperature), arranged as a quasi-uniform grid with the mean separation between the APs given by r_0 (horizontal model resolution). The chemical state of each AP is defined by the mixing ratios of all relevant constituents. The transport of APs occurs in terms of the isentropic trajectories (pure advection) followed by a mixing procedure due to adaptive regridding of the APs. The grid adaptation frequency is given by $1/\Delta t$ with the length of the pure advection Δt being a free parameter of the model with typical values ranging from 6 to 24 hours.

[12] The mixing intensity in CLaMS-2d is driven by the horizontal deformations in the flow and controlled by the critical Lyapunov exponent λ_c (see Figure 1). *Konopka et al.* [2003] compared CLaMS-2d simulations with in situ aircraft measurements of tracers observed at the edge of the northern polar vortex and estimated to be $\lambda_c \Delta t \approx 1$ for $r_0 = 45$ km and Δt ranging between 6 and 24 hours.

[13] CLaMS-3d generalizes both the advective part of transport and the isentropic mixing procedure to a full 3-D description. In particular, the cross-isentropic velocities of APs, $\dot{\theta} = d\theta/dt$, are derived from the radiation module based on the Morcrette scheme [*Morcrette*, 1991; *Zhong and Haigh*, 1995]. The heating/cooling rates, $\dot{T} = dT/dt$, are calculated in pressure coordinates for a cloud-free atmosphere using temperature profiles from meteorological data sets (here UKMO or ECMWF) and ozone/water vapor profiles from zonally and monthly averaged 10 years HALOE climatology (J.-U. Grooß et al., manuscript in preparation, 2004). To distinguish between vortex and extravortex ozone/water vapor profiles, the equivalent latitude is used as the horizontal coordinate in the (zonally symmetric) HALOE climatology. To take into account the impact of ozone depletion in the vortex on the radiation balance, the climatological profiles are replaced, if sufficiently high date coverage is available, by the profiles averaged only over the actual month of the year in question. Furthermore, a constant mixing ratio of CO_2 of 355 ppmv is assumed. The values of $\dot{T}$ are transformed to $\dot{\theta}$ through $\dot{\theta} = (\theta/T)\,\dot{T}$.

[14] The results of 3-D trajectory calculations are shown in Figure 2 where averaged diabatic descent of an ensemble of trajectories (black lines) starting and ending in the vortex is shown for the time period between 1 December 1999 and 20 March 2000.

[15] Following the general pattern observed in the last 10 years [*Rosenfield and Schoeberl*, 2001], the APs descend fastest in the fall while in springtime the descent rates decrease with decreasing altitude. *Greenblatt et al.* [2002] studied the descent of N_2O-isopleths in the range of 50–250 ppbv N_2O, corresponding to an altitude range of about 400 to 600 K. For the early vortex (26 November 1999 to 27 January 2000) they found an averaged descent rate of 0.82 K ± 0.20 K/day. Later, from 26 February to 12 March, the average descent rate decreased to 0.10 ± 0.25 K/day. The descent rates derived from CLaMS-3d trajectories starting at 500 K in Figure 2 amount to 0.97 K/day and 0.17 K/day for December/January and February/March, respectively. The best agreement with the experimental data (see next section) was achieved with the ECMWF
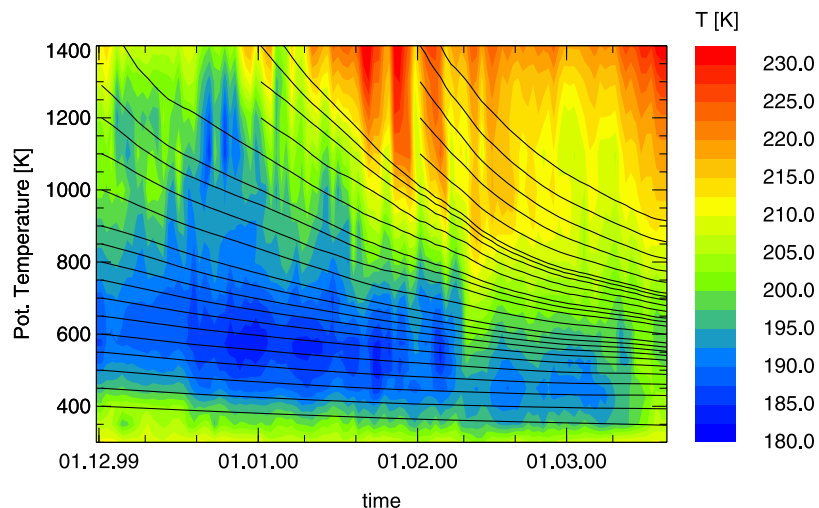
Figure 2. Mean diabatic descent of trajectories (black lines) within the vortex derived from ECMWF winds and cross-isentropic velocities calculated with the radiation module [*Zhong and Haigh*, 1995] based on the *Morcrette* [1991] scheme. (During the time periods and in the altitude regions where vortex is not present, we define the vortex air masses as APs with PV values larger then 80% of the maximal PV in the considered altitude.) The colors denote the minimum temperature northward of 45° calculated for the time period between 1 December 1999 and 20 March 2000.

temperature profiles and the monthly mean profiles of ozone. By using UKMO temperatures and monthly ozone profile averaged for each month over 10 years, the total descent of the vortex air calculated from 1 December to the beginning of March was underestimated by 20 K and 10 K, respectively.

[16] Now we discuss the 3-D generalization of the isentropic mixing procedure. As the vertical coordinate, we apply the altitude coordinate z and transform this coordinate to the potential temperature θ. In particular, we arrange the APs into n layers, extending between z_{min} and z_{max} or θ_{min} and θ_{max}, each layer with the thickness Δz_i or $\Delta\theta_i$, $i = 1\ldots n$ (see Figure 3). Assuming $p = p_0\exp(-z/H)$, with $H = 7$ km and an isothermal atmosphere in each layer, the thickness $\Delta\theta$ can be derived from Δz from $\ln(1 + \Delta\theta/\theta) = (\Delta zR)/(c_pH)$, where R, c_p, and θ denote the gas constant, the specific heat at constant pressure, and the potential temperature of the lower edge of the layer, respectively.

[17] At the initialization time $t = t_0$, the layers contain the same number of APs with the mean horizontal separation between the APs being given by r_0. In each layer, the APs are approximately uniformly distributed (vertically staggered) over the thickness of the layer. The mean vertical separation within the i-th layer is given by $\Delta z_i/2$ with the corresponding aspect ratio $\alpha_i = 2r_0/\Delta z_i$.

[18] In this paper we define the layers by setting $\alpha =$ const. Alternatively, we can use the condition that each layer contains the same mass of air. Assuming that r_0 is a given constant parameter, both conditions imply that the choice of the thickness of one layer determines the thickness of the other layers. Thus while in the first case $\alpha =$ const defines all the layers, in the second case Δz_1 or $\Delta\theta_1$ or $\alpha = \alpha_1 = 2r_0/\Delta z_1$ determines the nonuniform partition of the vertical axis through the conditions $\rho_i\Delta z_i = \rho_1\Delta z_1$, $i = 1\ldots n$, with $\rho_2 = \rho_1\exp(-\Delta z_1/H)$.

[19] From their initial positions, the APs are advected during a time step Δt (that for typical applications varies between 6 and 24 hours) to new positions according to the 3-D trajectories described above. These new AP positions, i.e., their latitudes, longitudes, and potential temperatures are shown schematically in Figure 4. According to their new θ-values, the APs are collected into the predefined layers of thickness $\Delta\theta$ discussed above, and in each layer the dynamically adaptive regridding procedure is carried out [*McKenna et al.*, 2002b]. In particular, the critical Lyapunov exponent λ_c and the time step Δt are chosen with the same values in every layer.
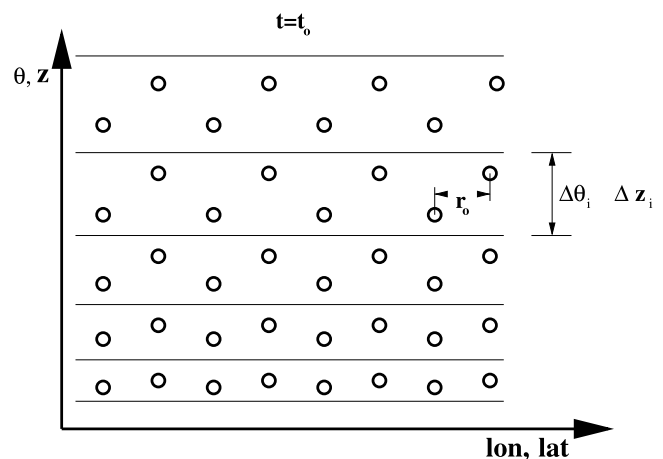
Figure 3. Initialization of CLaMS-3d. The APs are arranged in n layers, each layer with the thickness given by Δz_i or $\Delta\theta_i$, $i = 1\ldots n$. At the initialization time $t = t_0$, the layers contain the same number of APs. In each layer the APs are quasi-uniformly distributed (vertically staggered), i.e., without any significant variation of their spatial density. The mean horizontal and vertical separations between APs are given by r_0 and $\Delta z_i/2$, respectively. The corresponding aspect ratio of the i-th layer is given by $\alpha_i = 2r_0/\Delta z_i$.
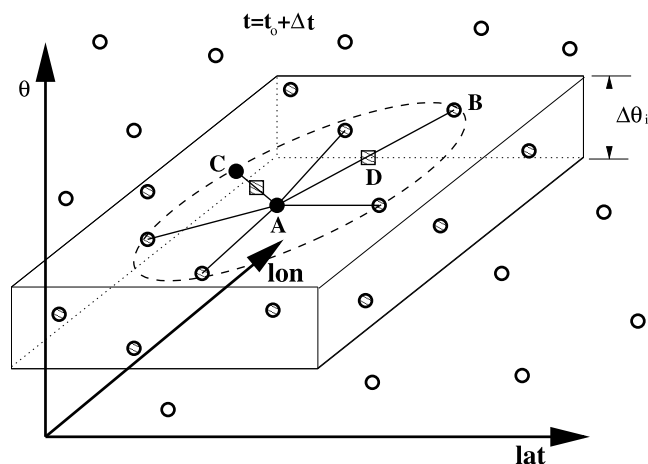
Figure 4. Schematic demonstration of mixing in CLaMS-3d. After the advection step Δt, the APs are collected into layers. Here all APs with θ values belonging to the layer $\Delta\theta_i$ are hatched. Then, in the same way as in the 2-D approach, sufficiently strongly deformed parts of the grid undergo regridding. In particular, a circle around a AP is deformed into a slanted ellipse. To find the sufficiently highly deformed parts of the grid, the distances of each AP to its nearest neighbors are calculated for the APs positions before the advection step and compared with those after the advection step Δt (solid lines around point A). Thus some grid points like B move further away while some like C move closer. In the same way as described by *McKenna et al.* [2002b], AB exceeds a critical horizontal separation r_+^c and a new grid point D is inserted (insertion). Conversely, the distance AC falls below a critical horizontal separation r_-^c and the grid points A and C are removed and a new grid point is introduced midway between the positions of A and C (merging). The numerical diffusion of the horizontal and vertical interpolations, used for calculation of the mixing ratios on the new (inserted and merged) APs is interpreted as mixing between the contributing APs.

[20] Thus the critical horizontal separations $r_\pm^c$ determining grid positions where APs are merged or new APs are inserted into the grid are given by $r_\pm^c = r_0 \exp \pm \lambda_c \Delta t$. To find deformed grid regions in the layer, the nearest neighbors (NN) are calculated from the horizontal positions of the APs before the advection step Δt by using the 2-D Delaunay triangulation technique [e.g., *Preparata and Shamos*, 1985]. Then the horizontal distances between every AP and its former NN are determined after the advection step and compared with $r_\pm^c$.

[21] If the horizontal separation between a given AP and one of its former NN exceeds a critical distance r_+^c, a new grid point is inserted midway between those two APs. To maintain the density of the grid points below a given threshold, the new NN relationships are determined and nearest neighbor separations are calculated. All APs with horizontal distances below the critical distance r_-^c are merged into a new AP midway between the original APs. The position and the chemical properties of the new APs result as the mean (horizontal and vertical) values of the contributing APs and, consequently, the involved APs are (horizontally and vertically) mixed. This procedure is

repeated in every layer and after each advection time step Δt.

[22] Owing to the cross-isentropic velocities of the APs, their potential temperatures change over the course of the run and the APs can move from one layer to an adjacent layer. In order to mix not only within a particular layer but also between the adjacent layers, we alternate the definition of the layers after each time step Δt by shifting the original layers by half of the layer thickness. This procedure is shown schematically in Figure 5. Without using alternating layers, a clustering of the APs around the center of each layer occurs due to the fact that the θ values of the new APs are midway between the potential temperatures of the old APs.

[23] The chemical properties of the APs in the top and bottom layers have to be fixed by appropriate boundary conditions which may be redefined in the course of a model run. The handling of these APs is similar to the initialization procedure described by *McKenna et al.* [2002a] and depends on the number of species considered and data sets available. An example of boundary conditions for a pure tracer study is discussed in the next section. For short time studies such as those discussed here, the impact of boundary conditions can be minimized by shifting the top and bottom layers sufficiently far away from the domain of interest.

[24] Now, the mass conservation of the proposed transport scheme is described in Figure 6 by using CLaMS-3d in pure tracer mode. Here, the relative change of the total mass calculated for CH_4 is shown over a time period of 3.5 months. To avoid the impact of mass fluxes through the boundaries, the results from calculations on a global domain are shown for two configurations of APs. In the 3-D case, the described alternating layers are used whereas in the 2-D studies the APs are arranged exactly on isentropic layers. The pure advection studies were carried out by switching off the mixing procedure. The mass of each AP was calculated from its density (derived from its pressure and temperature) and its volume defined as a product of the area of the 2-D Voronoi polygon containing the given AP in
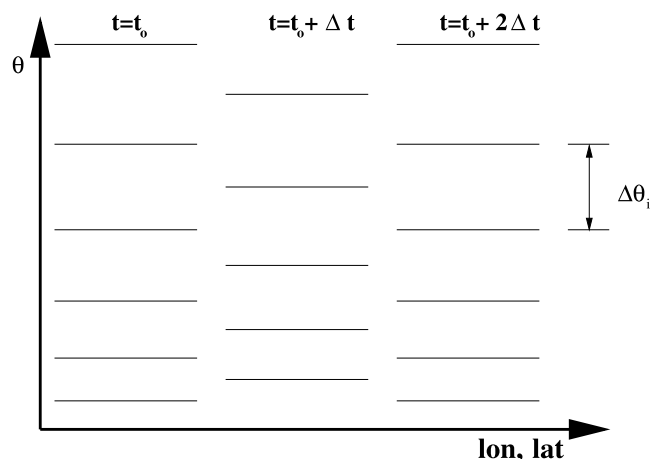
Figure 5. Alternating layers allow vertical mixing between the layers and avoid some clustering of the APs around the center of each layer due to excess vertical diffusion.
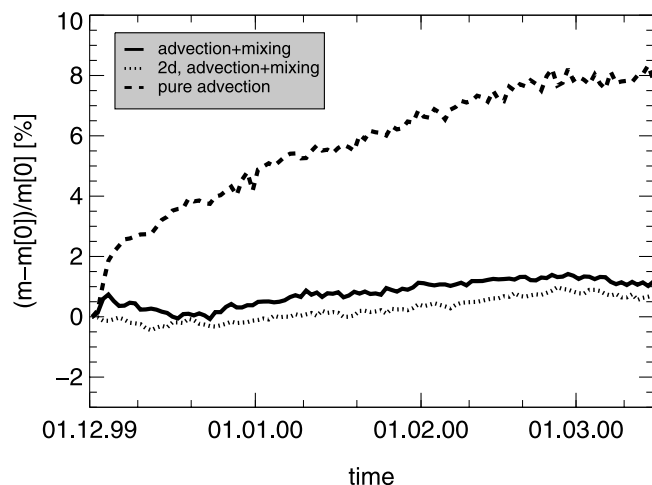
Figure 6. Mass conservation of the transport scheme calculated for CH_4. Mixing improves the mass conservation of chemically passive tracers by avoiding unrealistic clustering or dispersion of the initially quasi-uniform distribution.

the layer (calculated from the 2-D triangulation of all APs in the layer) and the thickness of the layer. The results show that the mixing scheme improves the mass conservation by avoiding unrealistic clustering or dispersion of the initially quasi-uniform distribution.

[25] Finally, we discuss how the concept of the deformation-induced CLaMS-2d mixing works in the 3-D version of the model. In particular, we consider an isentropic snapshot of the 2-D and 3-D version of the model by plotting the new points in the grid (i.e., places where mixing occurs) and the Lyapunov exponent λ quantifying the integral deformation in the flow. In Figure 7 the results at 700 K on 3 December 1999, i.e., after 3 days of integration, are shown. The pink dots mark the new APs which were added to the grid and, consequently, where mixing due to interpolations has occurred. For Δt and λ_c, the values 24 hours and 1.2 day^{-1} were used. The colors denote the Lyapunov exponent calculated from the deformation of a circle surrounding each AP. In the 3-D case the potential temperatures of the points defining the circle are uniformly distributed over the layer with $\Delta\theta = 25$ K. Thus the deformation of such a circle is driven by horizontal and vertical shear rates in the wind that are present on the horizontal and vertical scales r_0 and $\Delta\theta$, respectively. The slanted ellipse in Figure 4 shows schematically how the coupled horizontal and vertical deformation may deform a sufficiently small circle.

[26] The top panel of Figure 7 shows the results of 2-D transport where the positions of the new APs correlate with high horizontal deformations measured in terms of the finite time Lyapunov exponent λ. The lower panel shows a similar behavior in the 3-D case, i.e., mixing occurs predominantly in regions with high values of the Lyapunov exponent λ, this means in regions with high isentropic deformation rates. In addition, in the 3-D version of the model, high deformation of the flow and mixing can also be seen around the equator. Here, mixing can be explained by the contribution of the vertical shear in the convergence zone above the equator. Thus while in the isentropic case

only high horizontal deformations lead to high values of λ, in the 3-D case a combined effect of horizontal shear and vertical strain may cause high deformation rates.

3. Optimal Mixing: CLaMS-3d Simulations for Winter 1999−2000

[27] As described in the last section, mixing parameters in CLaMS-3d are defined by the grid properties, i.e., by the horizontal mean separation r_0 and the aspect ratio α and parameters controlling the deformation-induced mixing, i.e., the time step Δt determining the grid adaptation frequency $1/\Delta t$ and the critical Lyapunov exponent λ_c defining the flow regions with $\lambda > \lambda_c$, i.e., regions where significant mixing occurs.

[28] To find the best choice of these parameters, tracer transport studies of CH_4, Halon-1211, and ozone over the Northern Hemisphere were conducted between 1 December 1999 and 20 March 2000, i.e., for a time
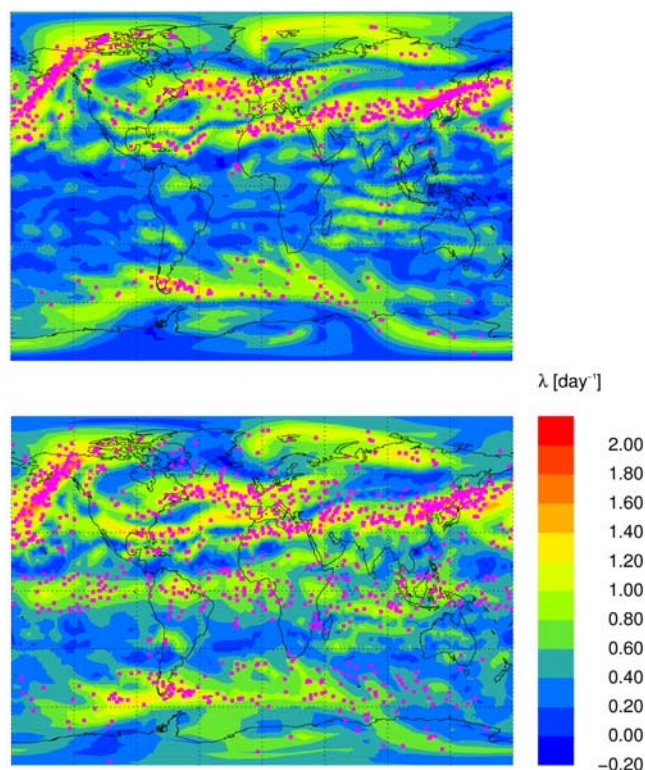
Figure 7. Deformation-induced mixing for CLaMS-2d (top) and CLaMS-3d (bottom) on 3 December 1999 at 700 K. The horizontal resolution is $r_0 = 100$ km. In the 3-D case the layer thickness is 25 K. The mixing parameters λ_c and Δt are 1.2 day^{-1} and 24 hours, respectively. The pink dots mark the new APs which were added to the grid by inserting and merging of APs. At these places, mixing due to interpolation has occurred. The colors denote the Lyapunov exponent λ calculated over the time step Δt from the deformation of a circle with a radius of 100 km surrounding each AP over the time step Δt. While in the isentropic case only high horizontal deformations lead to high values of λ, in the 3-D case a combined effect of horizontal strain and vertical shear causes high deformation rates.

period for which a very extensive data set of the SOLVE/THESEO-2000 campaign is available.

3.1. Initialization and Boundary Conditions

[29] The CLaMS-3d initial configuration of APs extends vertically between 350 and 1400 K. In each layer, the APs cover the Northern Hemisphere with high and low horizontal resolution r_0 northward and southward of 40°N, respectively. In the high-resolution region, several cases with different spatial resolution are considered with r_0 = 50, 100, 150, 200, and 300 km. In the low-resolution region, for the first four cases r_0 = 200 km is assumed and in the last case we set r_0 = 300 km. Model runs were made with the aspect ratio α varying between 100 and 1000. To study the influence of mixing, the grid adaptation frequency $1/\Delta t$ and the critical Lyapunov exponent λ_c were varied between 6–48 h^{-1} and 0.8–∞ day^{-1}, respectively, with $\lambda_c = \infty$ meaning pure advective transport without mixing.

[30] The initial distribution of CH_4 on 1 December is derived from the Mainz 2-D model [*Grooß*, 1996] together with HALOE and OMS observations that correct the Mainz 2-D CH_4 distribution in the midlatitudes and the vortex, respectively, due to too weak diabatic descent in the 2-D model. In particular, OMS profiles on 19 November (in situ) [*Ray et al.*, 2002] and 3 December (remote) [*Toon et al.*, 1999; *Salawitch et al.*, 2002] are taken into account. These profiles are shown in Figure 12. Here, the potential temperatures of the OMS profile from 19 November were transformed with the 3d forward trajectories to 3 December. Despite an overall good agreement between these two profiles, discrepancies can be seen in the altitude range between 18 and 22 km. On 3 December the sampled air parcels in this altitude range cover low values of the equivalent latitude and indicate that an intrusion from the midlatitudes has probably influenced the air masses in this region. Thus in the altitude range between 18 and 22 km, the OMS profile from 19 November seems to be more representative for the vortex air than the OMS data from 3 December.

[31] The Halon-1211 mixing ratios are initialized by use of the nonlinear CH_4/Halon-1211 correlation measured in the vortex during the OMS in situ flight on 19 November 1999 [*Ray et al.*, 2002]. The initial distribution of ozone in the vortex is derived from CH_4/ozone correlations obtained from the OMS in situ observations [*Müller et al.*, 2002]. This leads to nearly constant ozone in the vortex ($\approx$3 ppmv) between 500 and 800 K at the beginning of December [*Kawa et al.*, 2002]. The vortex edge is determined by the maximum PV gradient [*Nash et al.*, 1996]. Furthermore, two correlations are used in order to distinguish between the high-latitude and low-latitude extravortex air (see dashed lines in Figure 15) and, consequently, the ozone mixing ratios of APs outside the vortex are defined by a weighted mean of these two extravortex air correlations. To determine the dilution of vortex air due to intrusions of midlatitude air into the vortex, an artificial, digital tracer is transported. At the beginning of the simulation this tracer is initialized inside the vortex with the value 1 and with 0 elsewhere.

[32] The boundary conditions at the top and bottom layers are applied after each time step Δt and are derived from the PV/CH_4 and tracer-tracer correlations valid for the initialization time. These correlations often vary with the season and are often not well known. In the study presented here, the boundary conditions for CH_4 are determined from such a correlation and the actual PV in the respective layer. Backward trajectory calculations show that at the beginning of March the top layer around 1400 K has the strongest impact on the tracer distributions above 800 K and has little impact on the conditions below.

3.2. Validation of the Mixing Procedure

[33] To validate the mixing procedure in CLaMS-3d, the results of the model runs are compared with experimental data from late winter 2000, i.e., with OMS in situ for 5 March, OMS remote for 15 March, and with in situ observations by the Argus and ACATS instruments flown on the ER-2 between 20 January and 12 March [*Newman et al.*, 2002]. An example of the comparison between the ER-2 time series and the corresponding CLaMS-3 simulations with different mixing intensities is shown in Figure 8. Here, results for three different configurations of the mixing parameters: no mixing, optimal mixing, and excess mixing are plotted for two flights on 11 March (top) and 7 March (bottom). On 7 March the ER-2 encountered a filament of extravortex air near Spitzbergen (see Figure 9), whereas on 11 March an elongated filament of vortex air was encountered twice near the vortex edge over Scandinavia (see Figure 10).

[34] In the top panel of Figure 8 the high-resolution CH_4 time series measured by the Argus instrument with a frequency of about 0.3 Hz enable small-scale horizontal structures of up to several hundreds of meters to be resolved. In particular, a filament encountered twice near the vortex edge can be clearly seen in the shaded area of Figure 8. By comparing these fine-scale structures with CLaMS-3d simulations, we conclude that simulations without mixing produce much higher variability in the simulated fields than that observed. Alternatively, excess mixing smoothes out the filaments and underestimates the diabatic descent in the vortex due to excess vertical diffusivity.

[35] In the bottom panel of Figure 8 the comparison between the modeled and observed nonlinear CH_4/Halon-1211 correlations is shown for the flight on 7 March. Studying the impact of mixing on such nonlinear tracer-tracer correlations inside the vortex, [*Michelsen et al.*, 1998] and [*Plumb et al.*, 2000] suggested that signatures of mixing across the vortex edge, so-called anomalous mixing, may be detected in compact but nonlinear tracer/tracer relations. Comparing the modeled and observed correlations, it seems at first that mixing does not improve the agreement between the experiment and the CLaMS-3d simulations at all, i.e., that the zero mixing transport gives the best results. However, the discrepancies between the observed CH_4/Halon-1211 pairs and the corresponding simulations can be very large even in the zero mixing case when the APs do not change their composition and, consequently, must "stay" on their initial correlation curve. The green lines in the bottom panel of Figure 8 show such an example where the distance in the CH_4/Halon-1211-space between one observation and its corresponding simulation is smallest for the optimal mixing parameters and rather large for both the "zero mixing" and the "excess mixing" case.

[36] Thus the effect of "missing mixing" manifests itself in the fact that with increasing simulation time tracer
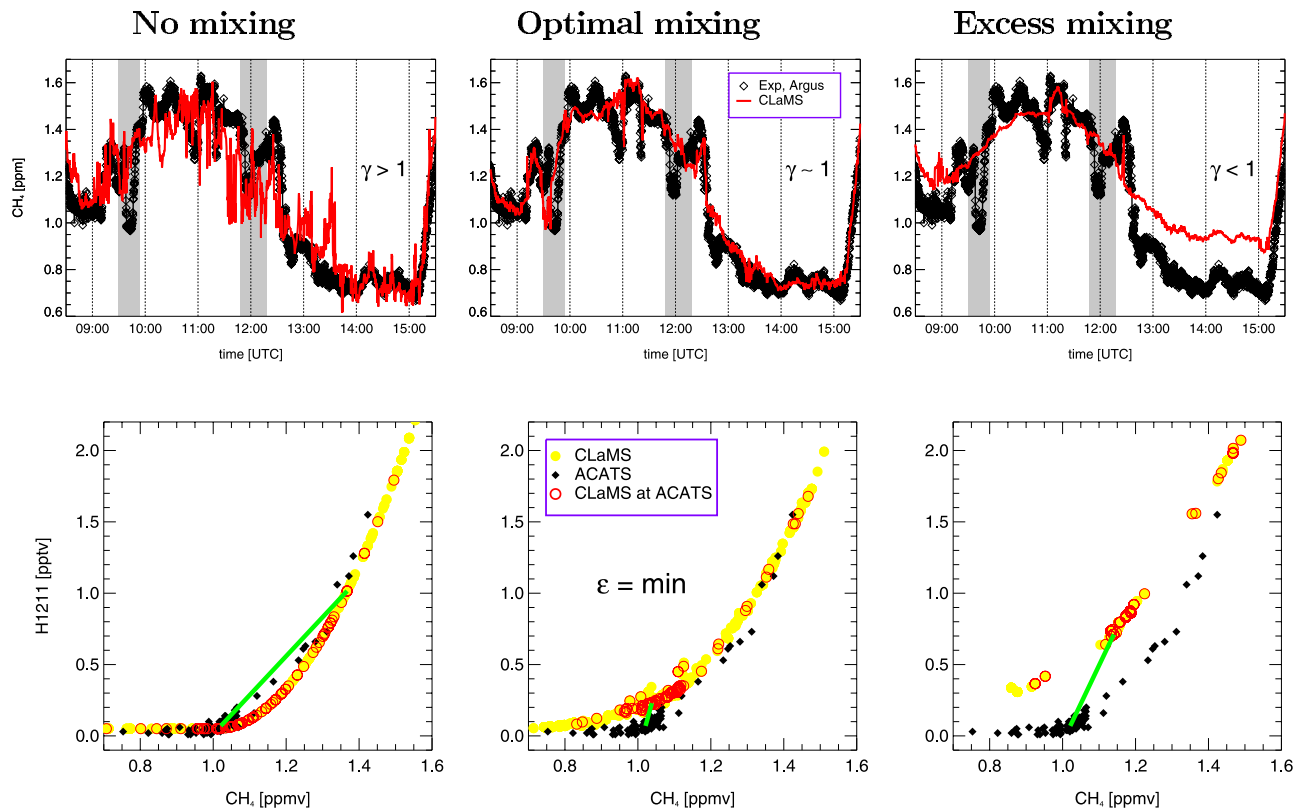
Figure 8. CLaMS-3d for different intensities of mixing versus observations along the ER-2 flight tracks on 11 March (top) and 7 March (bottom). The upper panel shows the high resolution Argus data of CH_4 (black diamonds) observed during a flight crossing an elongated filament near the vortex edge (shaded regions). In the lower panel, the nonlinear CH_4/Halon-1211 correlation measured with the ACATS instrument on 7 March during a flight within the vortex (black diamonds) is compared with CLaMS-3d (yellow filled circles represent CLaMS-3d along the flight track; red open circles represent CLaMS-3d sampled at the same location in the model as the ACATS observations). In the CH_4/Halon-1211-space, the green line connects a single observation with its corresponding CLaMS-3d simulated value (see text for a more detailed explanation).

distribution become too "grainy and spotty" and show too high spatial variability and too large deviations of the calculated tracer values from the corresponding observations. Only a small part of this effect is due to the errors in the wind fields, which cause spatial deviations between the positions of the observed and the calculated filaments. The most important reason for "too grainy and spotty" fields is the chaotic advection that, e.g., transports APs across the vortex edge which are not homogenized with their environment if mixing is too weak. This effect dominates the tracer distributions after more than 4 weeks of simulation.

[37] To optimize both the variability of the time series and the deviation from the nonlinear tracer-tracer correlations, we introduce the following two parameters:

$$\gamma = \frac{\Delta_{theor}}{\Delta_{exp}}, \quad \text{with} \quad \Delta = \sum_{i=1}^{m-1} |(f_{i+1} - f_i)| \qquad (1)$$
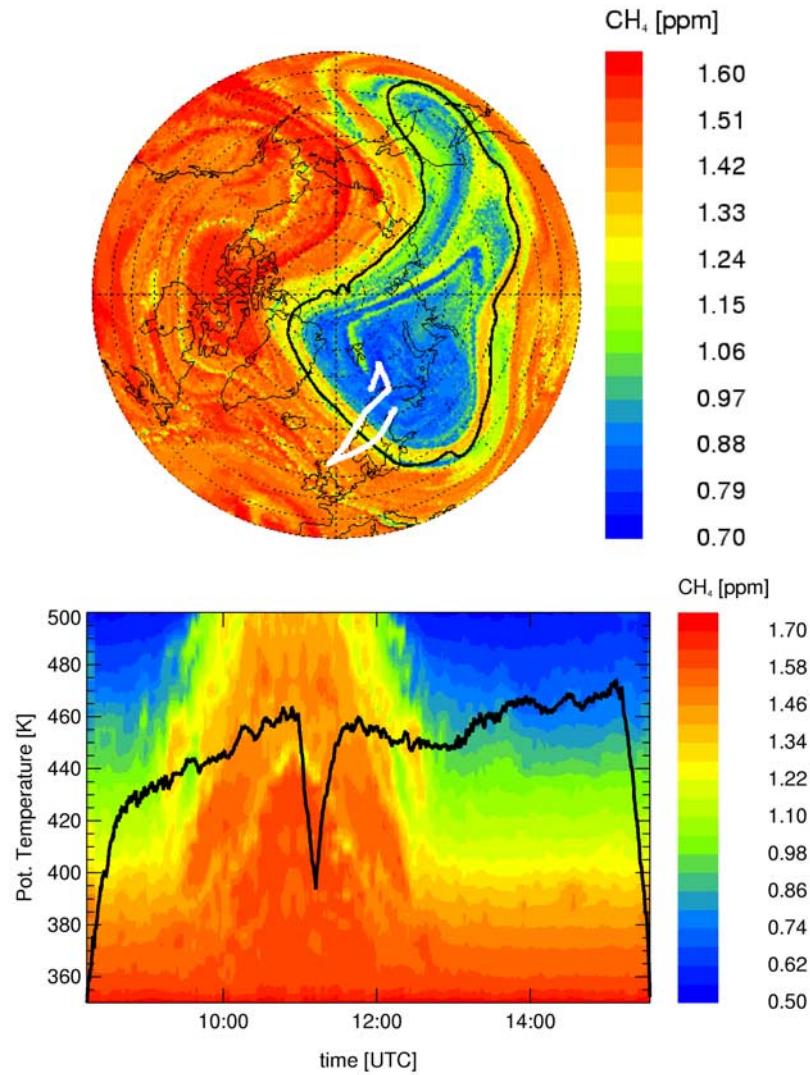
and

$$\epsilon^2 = \frac{1}{m} \sum_{i=1}^{m} \epsilon_i^2, \qquad (2)$$
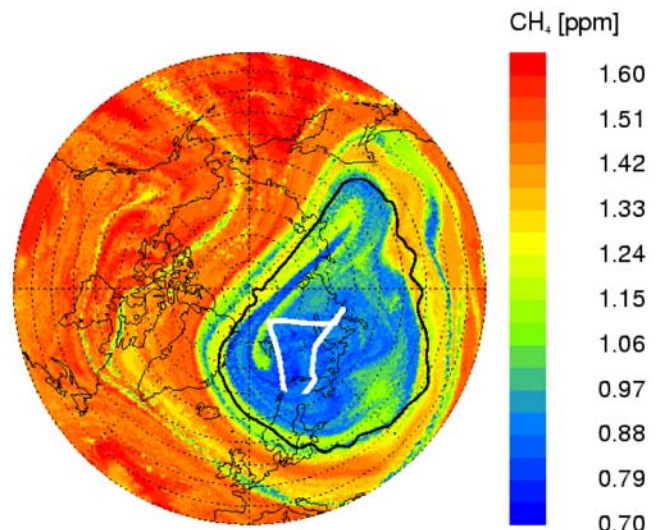
Figure 9. CLaMS-3d distribution of CH_4 at $\theta = 450$ K on 7 March with the ER-2 flight track transformed to the synoptic time 12 UCT (white line). Near Spitzbergen, the ER-2 touched a filament with extra-vortex air. For the calculation the optimal mixing parameters were used. The black line is the vortex edge [Nash et al., 1996].

Figure 10. CLaMS-3d distribution of CH_4 at $\theta = 450$ K on 11 March (top) and at the vertical cross section containing the ER-2 flight track (bottom). The black line in the bottom panel denotes the flight track. In both panels the filamentary structure of the vortex edge can be clearly seen.

with

$$\epsilon_i^2 = \left(1 - \frac{f_i^{theor}}{f_i^{exp}}\right)^2 + \left(1 - \frac{g_i^{theor}}{g_i^{exp}}\right)^2.$$

Here, f_i and g_i, $i = 1 \ldots m$ are the observed (exp) or simulated (theor) time series for CH_4 and Halon-1211, respectively, with $f_i = f(t_i)$. Thus γ measures the accumulated (absolute) differences between the observed and simulated time series, i.e., the ability of the model to correctly describe the spatial variability of the tracer observed along the flight track. (To include the effect of statistical noise into the analysis, the quantity $|(f_{i+1} - f_i)|$ in equation (1) should be replaced by $|(f_{i+1} - f_i)| - \sqrt{(\sigma f_{i+1})^2 - (\sigma f_i)^2}$, where σ denotes the relative statistical uncertainty of the measurements or calculation. We set here $\sigma = 0$ because the statistical noise of the model calculations can hardly be determined and sensitivity studies show only a weak influence of this parameter on our results (for $\sigma < 5\%$)). The second parameter ϵ is a measure of the mean deviation of the simulated CH_4/

Halon-1211 pairs from the corresponding observations where for the ideal case $\epsilon = 0$ and $\gamma = 1$ is expected. Furthermore, $\gamma > 1$ ($\gamma < 1$) implies that the spatial variability of the modeled time series is larger (smaller) compared to observed variability.

[38] By varying the mixing parameters, we define an optimal choice (optimal mixing) when ϵ is minimized near $\gamma = 1$. The mean values of γ and ϵ calculated over all the ACATS observations between 20 January and 12 March 2000 are shown in Figure 11. Here, a constant aspect ratio $\alpha = 250$ was used and the values of λ_c, Δt, and r_0 were varied between $0.8 - \infty$ day^{-1} ($\infty \rightarrow$ pure advection), 6–24 hours, and 300–100 km, respectively. The colored solid lines represent simulations with a different choice of r_0 while the size of the points denotes the value of the product $\lambda_c \Delta t$.

[39] The results show that compared with the no-mixing case ($\gamma \approx 4$, $\epsilon \approx 0.1$), mixing improves the simulated tracer distributions only for sufficiently high spatial resolutions, i.e., r_0 better than 300 km. The optimal agreement was obtained for $r_0 = 100$ km ($\gamma \approx 1.3$, $\epsilon \approx 0.03$). Furthermore,
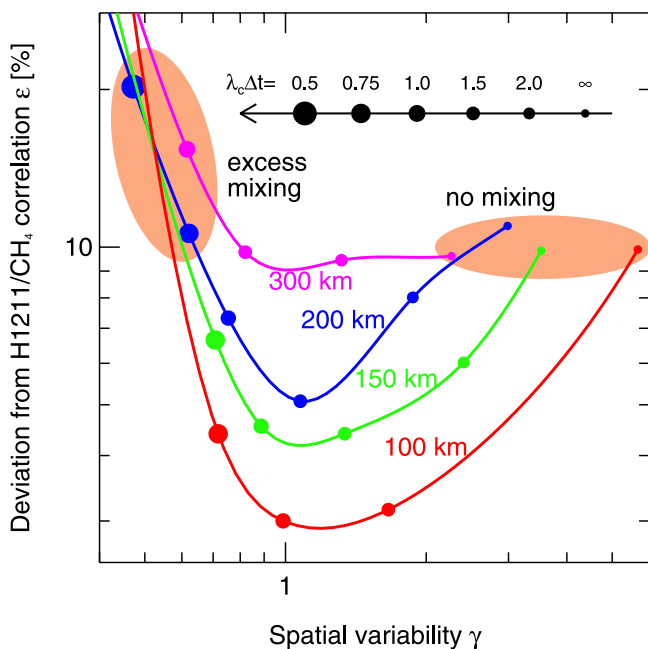
Figure 11. Optimizing of mixing parameters in CLaMS-3d. For a given horizontal resolution r_0, the best choice of the mixing parameters α, λ_c, and Δt is found by minimizing ϵ around $\gamma = 1$ (see text).

the level of this agreement depends on the product $\lambda_c \Delta t$ rather than on the particular parameters λ_c and Δt, with the optimal mixing given by $\lambda_c \Delta t = 1.5$. Similar sensitivity studies with respect to α (not shown) show that $\alpha = 250 \pm 100$ leads to a best description of the transport in the lower stratosphere.

[40] *Jost et al.* [2002] investigated the small-scale structures in the high resolved N_2O observation and concluded that from January to March 2000 in the 350–500 K potential temperature range, signatures of midlatitude air in the vortex were observed during 15% of the flight time on average and about 60% of these events occurred on flight segments shorter than 13 km. By repeating this statistical analysis with the time series derived from CLaMS-3d, we find that filaments wider than 40 km can be reproduced fairly well. Some of the filaments thinner than 40 km can also be found in CLaMS-3d simulations, although their contribution to the statistics strongly depends on the threshold defining the filaments and, consequently, is not easily distinguished from numerical noise in the model. Furthermore, the mean and smallest horizontal distances resolved by the current version of CLaMS-3d are of the order of $r_0 = 100$ km and $r_0 \exp - \lambda_c \Delta t = 20$ km, respectively. Thus we estimate 40 km to be the smallest scales for reliable horizontal variability resolved in the model.

[41] Finally, to give an impression of the quality of CLaMS-3d simulations, the comparison between the observed and simulated CH_4 time series for the OMS profile on 5 March and the ER-2 flight on 7 March are shown in Figure 12. A comparison of calculated profiles (red lines) with the balloon-borne data (black symbols) shows a general good agreement, although the model slightly overestimates some intrusions near 700 K. The discrepancy near 20 km on 3 December is caused by the intrusion that is not

captured by CLaMS-3d after 3 days of simulation. The comparison on 7 March along the ER-2 flight track shows that the model describes the observed CH_4 time series fairly well both with respect to the diabatic descent in the vortex and with respect to small-scale structures (filaments in the shaded areas).

4. Ozone Loss in the 1999–2000 Arctic Winter

[42] In this section we compare the ozone loss obtained from different studies for the 1999/2000 winter [*Newman et al.*, 2002; *Harris et al.*, 2002] with the results of CLaMS-3d inferred from the difference between the passive ozone transported with the model and in situ measurements. [*Goutail et al.*, 1999] applied this method to quantify the ozone loss from the difference between the column of passive ozone in a chemical transport model (REPROBUS initialized with POAM measurements) and the ozone columns as measured by SAOZ UV-visible network in the Arctic. *Hansen and Chipperfield* [1999] extended this
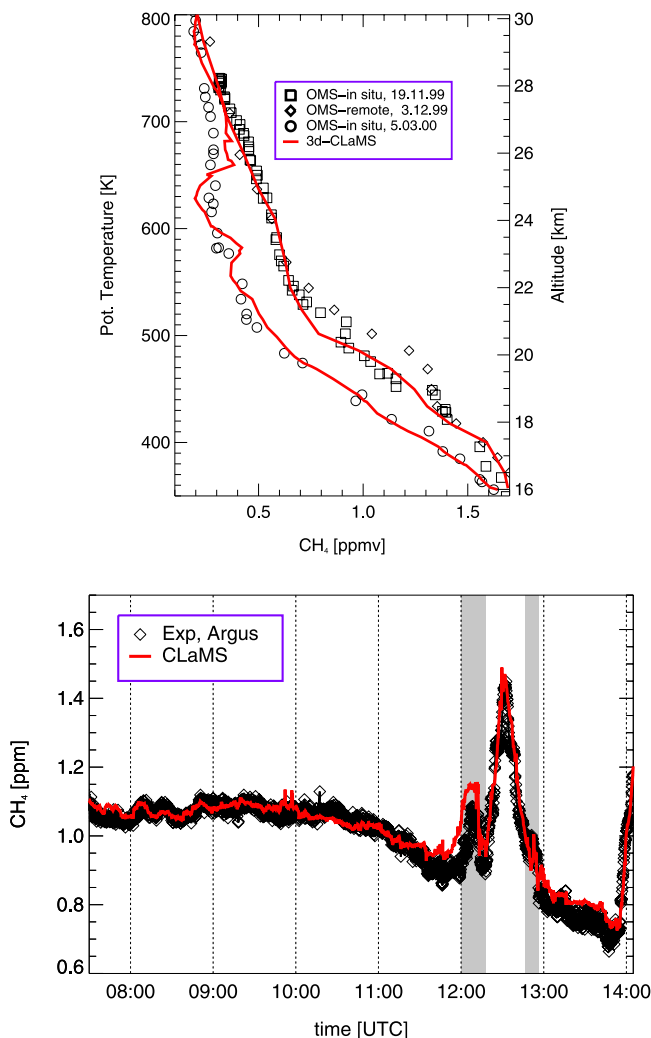
Figure 12. CLaMS-3d versus balloon (top) and aircraft (bottom) CH_4 observations on 5 and 7 March 2000, respectively. The OMS profiles on 19 November and 3 December were used for initialization of CLaMS-3d.
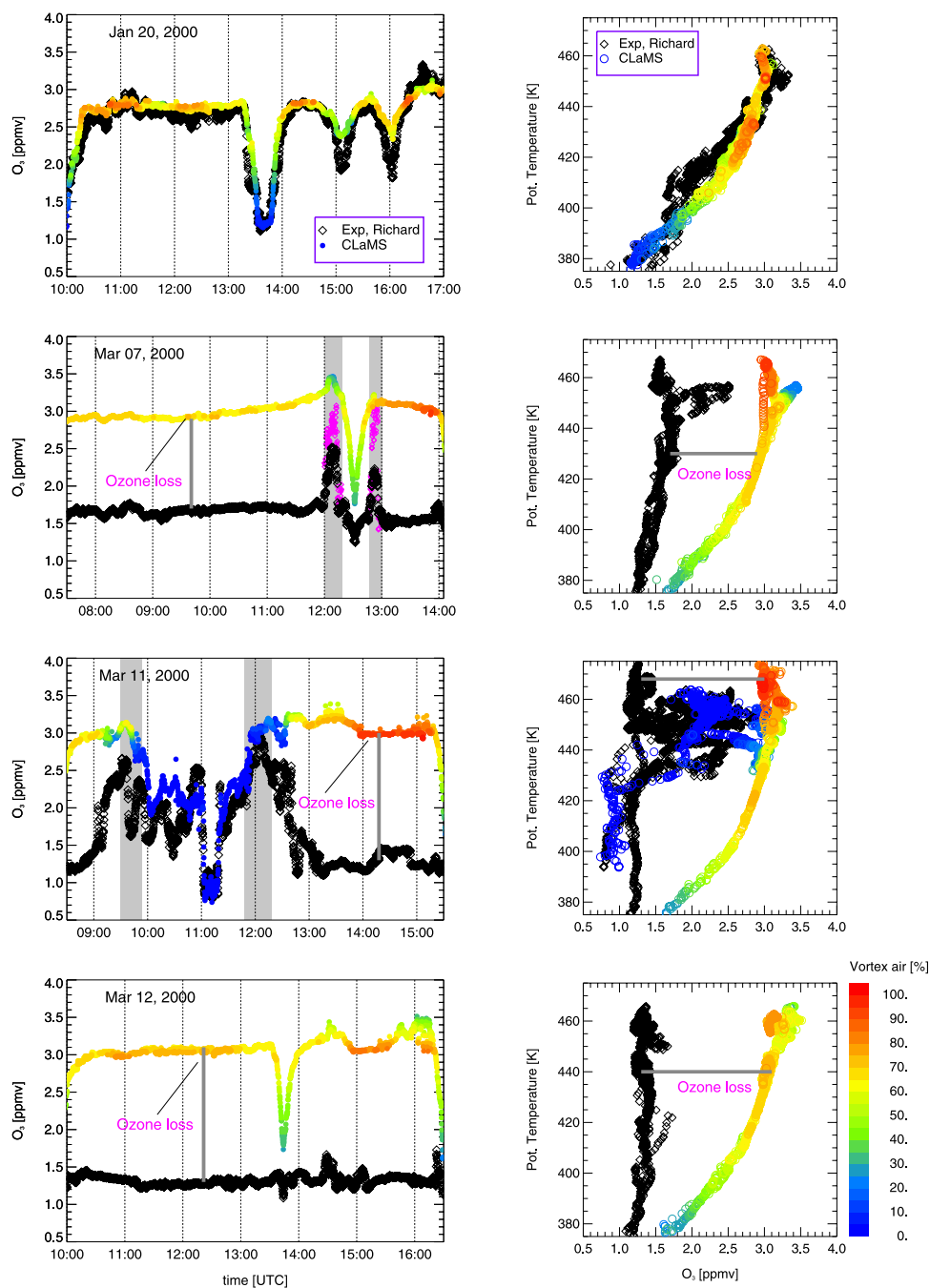
Figure 13. Ozone loss estimated from the difference between the CLaMS-3d passive ozone and ER-2 observations (black diamonds) [*Richard et al.*, 2001] on 20 January (top) and 7, 11 and 12 March (bottom) by taking into account time series (left) or profiles (right). The filled circles describe the passive ozone calculated from CLaMS-3d along the synoptic flight track, the colors denote the percentage of vortex air in these air masses. The pink diamonds in the shaded areas on 7 March represent the observation adjusted for the degree of dilution (see text for details).

method by considering the differences between the profiles instead of the columns.

[43] The left side of Figure 13 shows the comparisons on 20 January (top) and 7, 11, and 12 March (bottom) between the ozone time series observed on board the ER-2 [*Richard et al.*, 2001] and the tracer ozone along the flight track derived from CLaMS-3d simulations with optimal mixing parameters. On the right side of Figure 13, the corre-

sponding profiles are plotted. The colors of the simulated time series denote the percentage of pure vortex air within the sampled air masses. These values are derived from the interpolation of the advected and mixed artificial tracer (1 within and 0 outside of the vortex) along the aircraft track. Thus the colors quantify the dilution of the vortex air due to transport of the midlatitude air across the vortex edge.

[44] By taking into account all the ER-2 flights, a clear increase of ozone loss over the course of the winter can be seen. The simulated ozone mixing ratios on 20 January lie within the uncertainties of the measurements, thus no conclusions on ozone loss before that date can be drawn. The ozone loss estimated between 1 December 1999 and 12 March 2000 at 450 K amounts to 1.9 ± 0.3 ppmv. That means that the observed ozone is only 40% of the expected ozone at this altitude (i.e., 40% of the chemically undisturbed passive ozone tracer). Furthermore, in the altitude range covered by the ER-2 flights, the highest ozone loss is found in air masses with the highest percentage of vortex air.

[45] An interesting feature of ozone loss can be found on 7 March within the filament discussed in the previous section (shaded regions in the second row of Figure 13). The differences between the observed (2.5 and 2.2 ppmv around 12 and 13 UTC, respectively) and simulated tracer ozone (around 3.2 ppmv) suggests that chemical ozone loss of 0.7 and 1.0 ppmv occurred in different parts of the encountered filament. The backward trajectories show that the filament under investigation was formed in the vicinity of the vortex edge around 1 March. Thus the observed differences of 0.7 and 1.0 ppmv cannot be explained as a pure chemistry effect on a timescale of 7 days because this would require ozone loss rates of the order of 100 ppbv/day that is at least higher by factor 2 than inferred from observations and simulations [Rex et al., 2002].

[46] By assuming that part of this apparent strong ozone loss is due to mixing between high ozone in the filament and low ozone in the surrounding vortex air, we estimate this effect by recalculating the ozone mixing ratios within the filaments for a case when mixing between the filament and the ambient air would not occur. The results of this procedure are shown by the pink diamonds and indicate that at least part of the apparent ozone loss can be explained by mixing. Thus in addition to the mixing effect, the remaining part of the difference between passive and observed ozone (i.e., between the black and pink diamonds) is due to chemical ozone loss that occurred at the end of February in the vortex edge region.

[47] Ozone loss can also be derived from a comparison of tracer ozone with balloon observations. In Figure 14, ozone profiles for the OMS-remote flight on 3 December 1999 and 5 March are shown. Whereas the CLaMS-3d profile on 3 December shows good agreement with the observation, the difference between the observed and simulated profile on 5 March (shaded region) is a clear signature of chemical ozone loss between 380 and 520 K with a maximum loss around 460 K of about 1.7 ppmv, i.e., of about 60% of the expected ozone mixing rates. Furthermore, the sampled vortex air masses above 520 K did not experience any significant ozone losses, despite the fact that these air masses were well-isolated from the extra-vortex air.
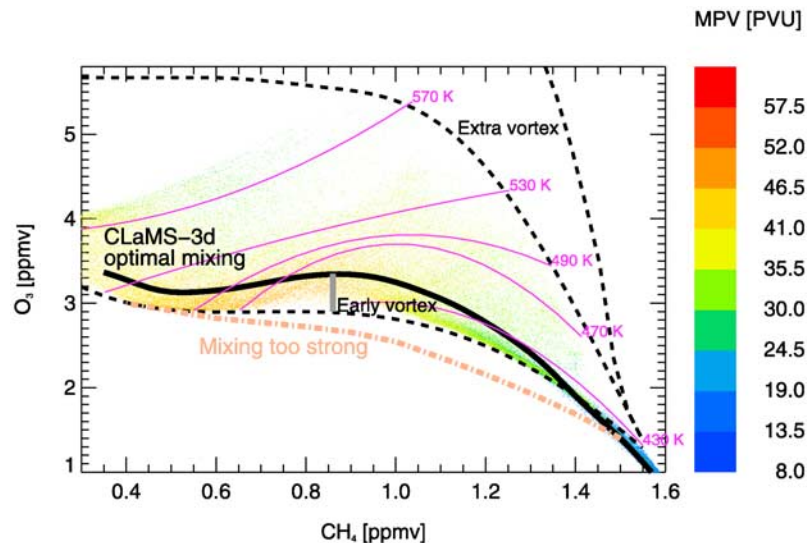
5. Impact of Mixing on Tracer/Ozone Correlations

[48] Correlations of ozone with simultaneous measurements of long-lived tracers (such as N_2O, CH_4, CO_2, HF) are often used to investigate chemical ozone loss in the polar vortex [e.g., Proffitt et al., 1990; Müller et al., 1997;
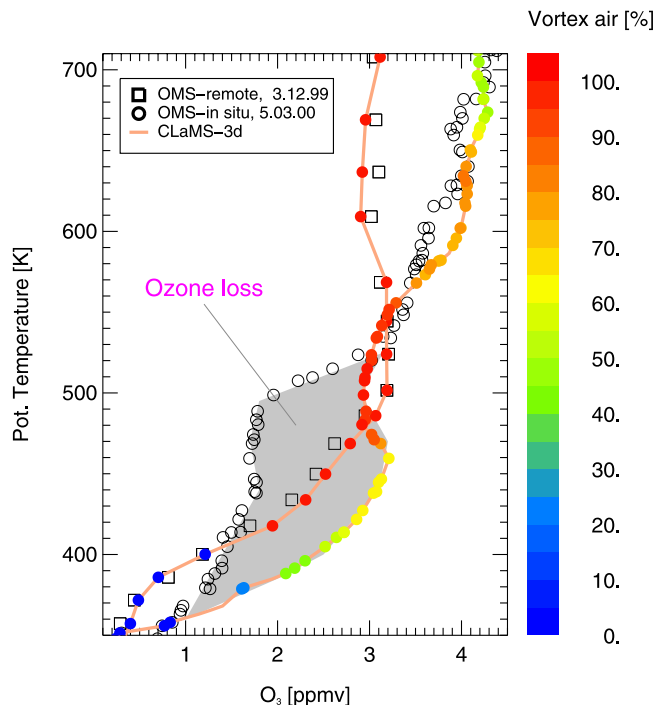
Figure 14. Ozone loss derived from the difference between the CLaMS-3d passive ozone and balloon observations (black symbols) on 3 December and 5 March. The colors indicate the dilution of the vortex air due to mixing between the midlatitude intrusions and vortex in the period between 1 December 1999 and the considered day.

Richard et al., 2001; Salawitch et al., 2002; Tilmes et al., 2003]. First, tracer/ozone correlations observed during late fall or at the beginning of the winter are considered as reference relations, representative of undisturbed "early vortex" conditions [Müller et al., 2001, 2002]. Thus assuming a well-isolated polar vortex and owing to the fact that the production of ozone during the polar night is negligible [Proffitt et al., 1993; Tilmes et al., 2003], the initial tracer relations are conserved towards spring until the returning solar light triggers the chemical ozone loss. Comparing the early vortex reference with spring measurements, possible deviations are interpreted as chemical ozone loss during the winter [e.g., Proffitt et al., 1990; Müller et al., 2002].

[49] However, such correlation can change, without chemical causes, due to mixing processes [Plumb et al., 2000]. Differential diabatic descent and subsequent homogenization inside the vortex [Ray et al., 2002] can modify the nonlinear tracer/ozone correlation in a way which may be erroneously interpreted as chemical ozone loss. However, there are no indications that this mechanism effects tracer/ozone relations during the period of strongest chemical ozone loss. On the other hand, mixing in of extra vortex midlatitude air after substantial chemical loss occurred inside the vortex can mask some of the loss. [Müller et al., 2001; Tilmes et al., 2003]. Figure 15 shows the influence of optimal CLaMS-3d mixing on the CH_4/ozone correlation within the vortex on 12 March, i.e., after more than 3 months of transport.

Figure 15. Impact of CLaMS-3d mixing on CH_4/ozone correlation. The black dashed lines describe the CH_4/ozone correlations as used for initialization of the model on 1 December 1999 (see section 3). The points correspond to the CH_4 and ozone mixing ratios of all CLaMS-3d APs on 12 March within the vortex covering the θ-range between 420 and 600 K. The APs with same θ values are connected with the solid pink lines. Along these lines, isentropic mixing occurs. The colors denote the modified PV of the APs, i.e., high PV values describe APs in the vortex core. The thick solid black line (best fit of all APs) is the new CH_4/ozone correlation. If a too strong mixing with too high vertical diffusivity is applied ($\alpha = 50$), the fit of the corresponding APs forms the beige dot-dashed line.

[50] Here, CLaMS-3d APs are colored with their modified PV values [*Lait*, 1994] with high and low values indicating core and edge regions of the vortex, respectively. In particular, only the APs within the polar vortex defined by the Nash criterion [*Nash et al.*, 1996] and with 380 K < θ < 600 K are plotted. The thin pink solid lines connect the APs with approximately the same θ-values and denote lines along which the isentropic mixing across the vortex edge has occurred. The black dashed lines are the CH_4/ozone correlation used for model initialization on 1 December 1999. As described in section 3, APs within the vortex are initialized with the early winter correlation (polynomial fit R8 in Table 1 given by *Müller et al.* [2002]), whereas for APs outside the vortex, the weighted contribution of two extra-vortex correlations is used which was derived from the HALOE observations described by *Müller et al.* [2002].

[51] In the optimal mixing case, about 20.000 APs describe the CH_4/passive ozone correlation within the vortex in the potential temperature range between 380 and 600 K. All the CH_4/ozone values lie above the early vortex correlation. To define a new CH_4/passive ozone correlation, we collect the APs into intervals (bins) with similar CH_4 values. The best fit connecting and smoothing the mean values within the bins (solid thick line) lies above the early vortex correlation. This is the consequence of isentropic mixing of the midlatitude air into the polar vortex [*Müller et al.*, 2001]. Only if unrealistically low values of the aspect ratio $\alpha \approx 50$ are used and, consequently, the tracer transport is dominated by too high values of the vertical diffusivity, does the best fit over all APs within the vortex lie below the early vortex correlation (beige dot-dashed line). Even in this case, however, the deviation from the reference curve is

much less than suggested in the conceptual model study of *Plumb et al.* [2000].

[52] Thus owing to the fact that the CH_4/ozone correlation inside the vortex is very different from the outside relation, the mixing between these two curves outweighs the effect of mixing along the lines crossing the curvatures of the particular CH_4/ozone correlations. This picture may be different if a universal, strongly nonlinear tracer/tracer correlation is valid both inside and outside the vortex [*Michelsen et al.*, 1998; *Plumb et al.*, 2000]. In such a case, mixing may occur along the mixing lines connecting the points of an universal tracer/ozone relation [*Michelsen et al.*, 1998].

[53] Thus the use of the early vortex correlation instead of the CH_4/passive ozone correlation inferred from CLaMS-3d as the reference to quantify the ozone loss in the winter and spring 2000 may lead to an underestimation on average of about 0.4 ppmv (the largest difference between the best fit derived from CLaMS-3d and the early vortex correlation). This value decreases to 0.1 ppmv if only air masses from the vortex core, with MPV > 45 PVU, are used for the calculation of the best fit (not shown).

6. Discussion and Conclusions

[54] The full 3-D version of CLaMS transport scheme was formulated and verified with the experimental data of the SOLVE/THESEO 2000 campaign for the period between 1 December 1999 and 20 March 2000. The 3-D Lagrangian mixing scheme introduced here is based on the layer concept that generalizes the CLaMS-2d isentropic mixing [*McKenna et al.*, 2002b] by including the vertical

shear within the layer that in addition to the horizontal strain, drives the intensity of mixing. Thus the regridding procedure in CLaMS-3d is driven by coupled horizontal and vertical deformations in the flow and controlled by the grid adaptation frequency $1/\Delta t$ and the critical Lyapunov exponent λ_c. The ratio between the horizontal and vertical diffusivity of the scheme is controlled by the aspect ratio α, i.e., by the ratio between the mean horizontal and vertical separations between the air parcels.

[55] The use of the staggered layers to determine the 2-D neighborhood relations between the APs instead of a full 3-D triangulation is mainly motivated by the fact that the horizontal and vertical scales are very different (α is of the order $\approx$250) and, consequently, have to be treated differently. For example, in the layer concept the vertical diffusivity of the APs during one mixing step is limited by the layer thickness and, consequently, prevents that some potential 3-D neighbors with too large vertical separation would mix. Furthermore, the numerical costs of the full 3-D triangulation exceed the costs of the layer-approach by the factor $n \approx 100$, where n denotes the number of layers. Also the 3-D triangulation of the boundaries can be avoided in the layer concept (note that a layer on a sphere has no boundaries).

[56] In CLaMS-3d, the cross-isentropic velocities are derived from a radiation module and are not coupled to the horizontal winds by the continuity equation. Because the vertical velocities are smaller than the horizontal winds by 3 orders of magnitude, the error of neglecting the continuity equation is comparable with the error in the meteorological winds. Consequently, the divergent parts of the flow are not distinguishable from the "numerical noise." Motivated by this property, the mixing procedure is based only on the non-divergent (i.e., area preserving) part of the flow by assuming $r_+ r_- = r_0^2$.

[57] By finding the best agreement between the simulated tracer distributions of long-lived tracers and the high-resolution in situ observations, the mixing parameters are optimized by choosing $\lambda_c \Delta t \approx 1.5$, $\alpha = 250$, and keeping mean horizontal separation r_0 between the APs smaller than 100 km (optimal mixing). For such high-resolution studies, about 3 million APs are used. Based on the Rossby ratio of the vertical and horizontal scales in quasi-geostrophic flows, *Lindzen and Fox-Rabinovitz* [1989] argued that the only consistent ratio between horizontal and vertical resolution, i.e., a consistent value of α, minimizes the numerical noise in the model. Studying the scale cascade in the lower stratosphere, *Haynes and Anglade* [1997] estimated $\alpha = 250$. Using the optimizing procedure described in this paper, $\alpha = 250$ could be confirmed with values between 200 and 300 leading to similar results.

[58] CLaMS-3d studies with optimal mixing parameters show that per day only about 10% of APs are affected by mixing. Furthermore, in addition to this temporal and spatial inhomogeneity, mixing in CLaMS-3d is characterized by a strong anisotropy. The product $\lambda_c \Delta t$ describes the (critical) eccentricity of an ellipse resulting from the deformation of a circle with a radius r_0 surrounding a given AP. Thus deformations exceeding the critical eccentricity switch on the regridding procedure and consequently mix the involved APs. The critical eccentricity of 1.5 means strong anisotropy of mixing with diffusivities along the wind exceeding the

diffusivities across the wind by the factor $(r_+^c/r_-^c)^2 = \exp(4\lambda_c\Delta t) \approx 400$.

[59] Sometimes it is useful to quantify mixing in terms of the mean (bulk) horizontal diffusivity [*Waugh et al.*, 1997; *Balluch and Haynes*, 1997]. Here we use the estimate $D_h \approx r_0^2/\Delta t$, with $r_0 = 100$ km and $\Delta t \approx 10$ days (i.e., by assuming that on average every AP is influenced by mixing after about 10 days). Then D_h is given by $1.2 \ 10^4 \ m^2 s^{-1}$. The vertical diffusivity D_v is smaller by a factor α^2 and is be $0.2 \ m^2 s^{-1}$. For the critical eccentricity of 1.5, the mean horizontal diffusivities along and across the wind are given by $2.3 \ 10^5$ and $5.7 \ 10^2 \ m^2 s^{-1}$, respectively.

[60] Even if CLaMS-3d shows the ability to reproduce small-scale structures with horizontal scales down to 40 km, the dissipation scales in the stratosphere, which are expected to be of the order 20 km [*Sparling and Bacmeister*, 2001], are probably not resolved by the model. The strong dilution rates near the lower boundary of the vortex (see, e.g., in Figure 14 the region below about 400 K) and too strong mixing noticeable in the nonlinear Halon-1211/CH_4-correlation (see Figure 8, optimal mixing) indicate that mixing in the model is still too strong. However, an increase of the model resolution to $r_0 = 50$ km does not significantly improve the comparison between the simulated and observed tracer field indicating that errors in the horizontal winds or in the cross-isentropic velocities have a greater impact than the errors in the mixing procedure.

[61] By comparing the simulated passive ozone distribution with the measured ozone profiles, the chemical ozone loss observed during the winter 1999/2000 was calculated. The derived ozone loss in the vortex between 1 December 1999 and the middle of March 2000 amounts to maximum values of about 1.9 ppmv around 460 K and agrees fairly well with the range of values estimated for this time period and altitude that vary between 1.5 and 2.3 ppmv [*Newman et al.*, 2002]. The advantage of the presented method is the high quality of the ozone tracer field that takes into account the diabatic descent in the vortex and mixing across the vortex edge.

[62] The study of the dilution of the vortex air due to intrusions of midlatitude air into the vortex indicates that the strongest ozone loss is present in the air masses with the highest percentage of the pure vortex air. Inversely, a strong isolation of air masses does not necessarily imply significant ozone loss as illustrated in Figure 14 near $\theta = 540$ K.

[63] Chemical ozone loss (deduced using a passive ozone tracer from a model) may be overestimated in air masses within the filaments of midlatitude air which are transported into and slowly mixed with the vortex air. The analysis of the ozone loss within the filament observed on 7 March shows that a significant part of the "apparent" ozone depletion in such air masses can be explained by mixing between the filament and strongly depleted air masses in the vortex. It should be emphasized that this is the opposite situation to the effect normally expected when mixing from outside the vortex tends to work against the effect of chemical ozone loss in the individual air masses inside the vortex. Consequently, in the presence of mixing the loss rates diagnosed (e.g., from the vortex average approach) would generally be smaller than the chemical loss rates.

[64] Finally, between 1 December and 20 March, mixing across the vortex edge that dilutes air masses within the

vortex occurs mainly isentropically. During this period, the impact of isentropic mixing across the vortex edge outweighs the effect of the differential descent on the tracer/ozone correlations in the vortex. CLaMS-3d tracer distributions within the vortex in December 1999 above 700 K show inhomogeneities that can be explained by differential descent of air in the vortex [*Ray et al.*, 2002]. The influence of this effect may be more significant in fall and early winter 1999 when strong inhomogeneities in both diabatic descent rates and tracer distributions are expected. The mixing-induced change of the early winter 1999 tracer/ozone correlations, which were used to determine the ozone loss, is about 0.4 ppmv on average with the smallest values in the vortex core of about 0.1 ppmv.

[65] Thus we conclude that using the early winter 1999 tracer/ozone correlation to determine the ozone loss in spring 2000, the ozone loss may be underestimated owing to the mixing effect by about 0.1 ppmv in the vortex core and by about 0.4 ppmv over the entire vortex. The underestimation of the ozone loss due to mixing would increase if mixing occurs after substantial ozone loss. To investigate this effect in detail, full chemistry simulations are necessary. An overestimation of ozone loss by using tracer/ozone correlation method can be excluded at least for this winter.

References

Balluch, M. G., and P. H. Haynes (1997), Quantification of lower stratospheric mixing processes using aircraft data, *J. Geophys. Res.*, *102*, 23,487–23,504.

Goutail, F., et al. (1999), Total ozone depletion in the Arctic during the winters of 1993–94 and 1994–95, *J. Atmos. Chem.*, *32*, 35–59.

Greenblatt, J., et al. (2002), Tracer-based determination of vortex descent in the 1999/2000 arctic winter, *J. Geophys. Res.*, *107*(D20), 8279, doi:10.1029/2001JD000937.

Grooß, J.-U. (1996), Modelling of stratospheric chemistry based on HALOE/UARS satellite data, Ph.D. thesis, Univ. of Mainz, Mainz, Germany.

Grooß, J.-U., et al. (2002), Simulation of ozone depletion in spring 2000 with the Chemical Lagrangian Model of the Stratosphere (CLaMS), *J. Geophys. Res.*, *107*(D20), 8295, doi:10.1029/2001JD000456.

Hansen, G., and M. P. Chipperfield (1999), Ozone depletion at the edge of the Arctic polar vortex 1996/1997, *J. Geophys. Res.*, *104*, 1837–1845.

Harris, N., M. Rex, F. Goutail, B. Knudsen, G. Manney, R. Müller, and P. von der Gathen (2002), Comparison of empirically derived ozone loss rates in the Arctic vortex, *J. Geophys. Res.*, *107*(D20), 8264, doi:10.1029/2001JD000482.

Haynes, P., and J. Anglade (1997), The vertical scale cascade in atmospheric tracers due to large-scale differential advection, *J. Atmos. Sci.*, *54*, 1121–1136.

Jost, H.-J., et al. (2002), Mixing events revealed by anomalous tracer relationships in the arctic vortex during winter 1999/2000, *J. Geophys. Res.*, *107*(D24), 4795, doi:10.1029/2002JD002380.

Kawa, S., R. Bevilacqua, J. Margitan, A. Douglass, M. Schoeberl, K. Hoppel, and B. Sen (2002), Interaction between dynamics and chemistry of ozone in the setup phase of the Northern Hemisphere polar vortex, *J. Geophys. Res.*, *108*(D5), 8310, doi:10.1029/2001JD001527.

Knudsen, B. M., et al. (1998), Ozone depletion in and below the Arctic vortex for 1997, *Geophys. Res. Lett.*, *25*, 627–630.

Konopka, P., J. U. Grooß, G. Günther, D. S. McKenna, R. Müller, J. W. Elkins, D. Fahey, and P. Popp (2003), Weak impact of mixing on chlorine deactivation during SOLVE/THESEO2000: Lagrangian modeling (CLaMS) versus ER-2 in situ observations., *J. Geophys. Res.*, *108*(D5), 8324, doi:10.1029/2001JD000876.

Lait, L. R. (1994), An alternative form for potential vorticity, *J. Atmos. Sci.*, *51*, 1754–1759.

Lindzen, R. S., and M. S. Fox-Rabinovitz (1989), Consistent vertical and horizontal resolution, *Mon. Weather Rev.*, *117*, 2575–2583.

McIntyre, M. E., and T. N. Palmer (1984), The 'surf zone' in the stratosphere, *J. Atmos. Terr. Phys.*, *46*, 825–849.

McKenna, D. S., J.-U. Grooß, G. Günther, P. Konopka, R. Müller, G. Carver, and Y. Sasano (2002a), A new Chemical Lagrangian Model of the Stratosphere (CLaMS): 2. Formulation of chemistry-scheme and initialisation, *J. Geophys. Res.*, *107*(D15), 4256, doi:10.1029/2000JD000113.

McKenna, D. S., P. Konopka, J.-U. Grooß, G. Günther, R. Müller, R. Spang, D. Offermann, and Y. Orsolini (2002b), A new Chemical Lagrangian Model of the Stratosphere (CLaMS): 1. Formulation of advection and mixing, *J. Geophys. Res.*, *107*(D16), 4309, doi:10.1029/2000JD000114.

Michelsen, H. A., G. L. Manney, M. R. Gunson, and R. Zander (1998), Correlations of stratospheric abundances of NO_y, O_3, N_2O, and CH_4 derived from ATMOS measurements, *J. Geophys. Res.*, *103*, 28,347–28,359.

Morcrette, J.-J. (1991), Radiation and cloud radiative properties in the European Centre for Medium-Range Weather Forecasts forecasting system, *J. Geophys. Res.*, *96*(D5), 9121–9132.

Müller, R., P. J. Crutzen, J.-U. Grooß, C. Brühl, J. M. Russell III, H. Gernandt, D. S. McKenna, and A. F. Tuck (1997), Severe chemical ozone loss in the Arctic during the winter of 1995–96, *Nature*, *389*, 709–712.

Müller, R., U. Schmidt, A. Engel, D. McKenna, and M. Proffitt (2001), The O_3/N_2O relationship from balloon-borne observations as a measure of Arctic ozone loss in 1991–1992, *Q. J. R. Meteorol. Soc.*, *127*, 1389–1412.

Müller, R., et al. (2002), Chlorine activation and chemical ozone loss deduced from HALOE and balloon measurements in the Arctic during the winter of 1999–2000, *J. Geophys. Res.*, *107*(D5), 8302, doi:10.1029/2001JD001423.

Nash, E. R., P. A. Newman, J. E. Rosenfield, and M. R. Schoeberl (1996), An objective determination of the polar vortex using Ertel's potential vorticity, *J. Geophys. Res.*, *101*, 9471–9478.

Newman, P., et al. (2000), An overview of the SOLVE-THESEO 2000 campaign, *J. Geophys. Res.*, *107*, 8259.

Plumb, R. A., D. W. Waugh, and M. P. Chipperfield (2000), The effect of mixing on tracer relationships in the polar vortices, *J. Geophys. Res.*, *105*, 10,047–10,062.

Plumb, R. A., W. Heres, J. L. Neu, N. M. Mahowald, J. del Corral, G. C. Toon, E. Ray, F. Moore, and A. E. Andrews (2003), Global tracer modeling during SOLVE: High latitude descent and mixing, *J. Geophys. Res.*, *108*(D5), 8309, doi:10.1029/2001JD001023.

Preparata, F. P., and M. Shamos (1985), *Computational Geometry. An Introduction*, Springer-Verlag, New York.

Proffitt, M. H., J. J. Margitan, K. K. Kelly, M. Loewenstein, J. R. Podolske, and K. R. Chan (1990), Ozone loss in the Arctic polar vortex inferred from high altitude aircraft measurements, *Nature*, *347*, 31–36.

Proffitt, M. H., K. Aikin, J. J. Margitan, M. Loewenstein, J. R. Podolske, A. Weaver, K. R. Chan, H. Fast, and J. W. Elkins (1993), Ozone loss inside the northern polar vortex during the 1991–1992 winter, *Science*, *261*, 1150–1154.

Ray, E. A., F. L. Moore, J. W. Elkins, D. F. Hurst, P. A. Romashkin, G. S. Dutton, and D. W. Fahey (2002), Descent and mixing in the 1999–2000 northern polar vortex inferred from in situ tracer measurements, *J. Geophys. Res.*, *107*, 8285.

Rex, M., et al. (2002), Chemical depletion of Arctic ozone in winter 1999/2000, *J. Geophys. Res.*, *107*, 8276.

Richard, E. C., et al. (2001), Severe chemical ozone loss in the Arctic polar vortex during winter 1999–2000 inferred from in-situ airborne measurements, *Geophys. Res. Lett.*, *28*(11), 2000–2197.

Rosenfield, J. E., and M. R. Schoeberl (2001), On the origin of polar vortex air, *J. Geophys. Res.*, *106*(D24), 33,485–33,497.

Salawitch, R., et al. (2002), Chemical loss of ozone during the Arctic winter of 1999–2000: An analysis based on balloon-borne observations, *J. Geophys. Res.*, *107*, 8269.

Sparling, L. C., and J. T. Bacmeister (2001), Scale dependence of tracer microstructure: PDFs, intermittency and the dissipation scale, *J. Geophys. Res.*, *28*(14), 2823–2826.

Tilmes, S., R. Müller, J.-U. Grooß, D. McKenna, J. Russell, and Y. Sasano (2003), Calculation of chemical ozone loss in the Arctic winter 1996–1997 using ozone-tracer correlations: Comparison of ILAS and HALOE results, *J. Geophys. Res.*, *108*(D2), 4045, doi:10.1029/2002JD002213.

Toon, G. C., et al. (1999), Comparison of MkIV balloon and ER-2 aircraft measurements of atmospheric trace gases, *J. Geophys. Res.*, *104*, 26,779–26,790.

Waugh, D. W., et al. (1997), Mixing of polar vortex air into middle latitudes as revealed by tracer-tracer scatterplots, *J. Geophys. Res.*, *102*, 13,119–13,134.

Zhong, W., and J. D. Haigh (1995), Improved broadband emissivity parameterization for water vapor cooling rate calculations, *J. Atmos. Sci.*, *52*(1), 124–138.

————————————

J. W. Elkins, NOAA Climate Monitoring and Diagnostics Laboratory, 325 Broadway R/CMDLI, Boulder, CO 80305, USA. (jelkins@cmdl.noaa.gov)

J.-U. Grooß, G. Günther, P. Konopka, R. Müller, and H.-M. Steinhorst, Forschungszentrum Jülich, Institute for Stratospheric Chemistry (ICG-1), 52425 Jülich, Germany. (j.-u.grooss@fz-juelich.de; g.guenther@fz-juelich.de; p.konopka@fz-juelich.de; ro.mueller@fz.juelich.de; h.steinhorst@fz-jeulich.de)

D. S. McKenna, National Center for Atmospheric Research, 1850 Table Mesa Drive, Boulder, CO 80307-3000, USA. (danny@acd.ucar.edu)

H.-J. Jost, NASA Ames Research Center, Mail Stop 245-5, Moffett Field, CA 94035-1000, USA. (hjost@mail.arc.nasa.gov)

E. Richard, Cooperative Institute for Research in Environmental Sciences, University of Colorado, Boulder, CO 80309, USA. (erik.c.richard@noaa.gov)

U. Schmidt, Institut für Meteorologie und Geophysik, Johann Wolfgang Goethe-University, Frankfurt am Main, Georg-Voigt Strasse 14, D-60325 Frankfurt, Germany. (uschmidt@meteor.uni-frankfurt.de)

G. Toon, Jet Propulsion Laboratory, Mail Stop 183-601, 4800 Oak Grove Drive, Pasadena, CA 91109-8099, USA. (toon@mark4sun.jpl.nasa.gov)